3D Printed Microneedles for Anticancer Therapy of Skin Tumours

Md Jasim Uddin[1,4], Nicolaos Scoutaris[1], Sophia N. Economidou[2], Clementine Giraud[3], Babur Z. Chowdhry[1], Dennis Douroumis[1,2*]

[1]Faculty of Engineering and Science, School of Science, University of Greenwich, Chatham Maritime, Chatham, Kent ME4 4TB, United Kingdom

[2]Medway School of Pharmacy, University of Kent, Medway Campus, Central Avenue, Chatham Maritime, Chatham, Kent, ME4 4TB, United Kingdom

[3]Polytech Marseille, Aix Marseille University, Filière Matériaux:Luminy Case 925-13288 Marseille Cedex 09, France

[4]Department of Pharmacy, BRAC University, Bangladesh. Address: 41 Pacific Tower, Mohakhali, Dhaka-1212, Bangladesh.

ABSTRACT

In this study, novel 3D printed polymeric microneedle arrays were fabricated for enhanced cisplatin delivery to A-431 epidermoid skin tumours for cancer treatment. The microneedles were built by selectively photopolymerising consecutive layers of a biocompatible photopolymer resin using stereolithography (SLA), followed by coating of cisplatin formulations using inkjet dispensing on the needle surface. The printability via SLA was optimized to improve microneedle mechanical properties and optical coherence tomography analysis showed excellent piercing capacity of 3D printed microneedles to an 80% penetration depth. Franz cell diffusion studies revealed rapid cisplatin release rates of 80-90% within 1 hr and *in vivo* evaluation with Balb/c nude mice presented sufficient cisplatin permeabilization with high anticancer activity and tumour regression. Histopathology analysis confirmed the tumour inhibition effect, showing demarcated lesions with thin fibrous capsules and necrotic cores. The use of 3D printed microneedles demonstrates the potential for *in-vivo* transdermal delivery of anticancer drugs.

KEYWORDS: 3D printing; stereolithography; microneedles; anticancer delivery; tumour regression.

INTRODUCTION

Over the last 20 years, microneedle (MN) devices have been extensively used for transdermal administration of various medicines in a non-invasive manner [1-3]. The miniature devices have shown a unique ability to facilitate the delivery of small drug molecules, RNA, DNA and vaccines by penetrating the stratum corneum and unloading the active substances directly to the dermis [4, 5]. Compared to passive skin drug delivery approaches, MNs act as a microinjection device, with a rapid increase of local drug concentration and, hence, enhanced systemic drug absorption and improved bioavailability. Clinical applications have shown that MNs do not stimulate nerves associated with pain and pierce the skin without causing infections or irritation, resulting in improved patient compliance. The application of MNs does not require a high level of expertise as they are self-administrated without generating medical sharps waste [6]. MNs are classified into five categories: solid, coated, hollow, hydrogel-forming and dissolvable microneedles which are usually made from metals, polysaccharides or polymeric materials [7].

Recent advances in the application of MNs to the skin involve the delivery of anticancer agents for the treatment of skin tumours. Jain et al., used metal microneedles coated with 5-aminolevulinic acid (5-ALA), a photosensitizer drug, for skin tumour treatment using photodynamic therapy [8]. The localized effect of MN doses, administrated at 1.75 mg, suppressed the growth of subcutaneous tumours by 57% while topical creams of 5-ALA did not have an effect, even when applied for several hours. Hao et al., [9], combined chemotherapy and photothermal therapy for the development of a PEGylated gold nanorod coated poly(l-lactide) microneedle system in order to enhance the antitumor efficiency of docetaxel-loaded MPEG-PDLLA micelles for the treatment of A431 tumours. By using low doses of docetaxel (5 mg/kg) and GNR nanorods, the A431 tumours were eradicated, showcasing

the synergetic effect on epidermoid cancer. In a very interesting study, poly(l-lactide) (PLLA) MNs were fabricated to develop "multilayer tattoo" DNA vaccines [10]. MNs were used for rapid implantation of vaccine-loaded polymer films carrying DNA, immune-stimulatory RNA, and biodegradable polycations into the immune-cell-rich epidermis. Multilayer tattooing enabled more efficient immune responses in mice compared to naked DNA injections or *in vivo* electroporation. In a similar work, Ali et al., [11], developed a smart technology platform for DNA vaccination for the treatment of cervical cancer. They condensed DNA into cationic nanoparticles by blending with the RALA peptide and polymeric MNs loaded with nanoparticles were used for DNA vaccination. The polymeric MNs protected DNA from degradation in the polyvinylpyrrolidone matrix and it was found that MN administration delayed TC-1 tumour initiation in a prophylactic model, slowed tumour growth and prolonged animal survival. Silicon biodegradable nanoneedles were applied for localised deliver of quantum dots to the surface of tissues. The nanoneedles achieved controlled access to the cytosol of a large cell population while they were able to deliver and sense the intracellular space [12].

However, the typical materials and manufacturing processes employed for the development of MNs present several disadvantages, that hamper the broader adoption of such systems for transdermal drug delivery. Micromoulding, is commonly used for the fabrication of dissolving and gel-forming MNs, is often time-consuming and difficult to scale-up for production, since it requires a number of sequential steps. Furthermore, traditional coating technologies do not always result in uniform, accurate and reproducible active coated layers and fail to avoid drug deposition on the MN substrate, resulting to drug waste and uncertainty regarding the exact loaded dosage. Moreover, there are serious concerns related to the biocompatibility and skin irritation of the materials used for MN fabrication (e.g. silicon, polymers), as most of them are suitable for oral use but not approved for transdermal delivery.

Another shortcoming of MN-mediated transdermal delivery is the limited drug loading, rendering them unsuitable for delivering large amounts of drug substances.

Since its introduction in the 1980s, 3D printing or Additive Manufacturing has revolutionised numerous fields including the biomedical, materials sciences and pharmaceutical since it allows the fabrication of elaborate structures fast, cost-effectively, accurately and reproducibly [13]. 3D printing consists of a range of technologies that employ various materials and physicochemical principals, under the common umbrella law that a physical object is created on the basis of a virtual Computer Aided Designed (CAD) model, through the fabrication of consecutive layers [13]. Among other 3D printing techniques, Stereolithography (SLA) enables the fabrication of the designed models via the consecutive layer-wise polymerization of UV-sensitive polymers, by using a curing process, namely photopolymerization [14 – 18]. The use of SLA for the fabrication of MNs was introduced by Gittard et al., [19] when they 3D printed MNs in various geometries for wound healing applications, which were then coated with silver and zinc oxide thin films via pulse laser deposition of. In another study, dacarbazine (1-2%), a skin anticancer drug, was incorporated into poly (propylene fumarate)/drug blends followed by photopolymerization using a micro-stereolithographic apparatus that fabricated the microneedle arrays [20].

Herein, we report, for the first time, the fabrication of 3D printed MN patches loaded with an anticancer drug substance for the treatment of skin tumours [21]. The 3D printed designs, termed cross–MNs, were made of a biocompatible polymer, followed by inkjet coating of cisplatin-polymeric layers on the MN surface. Embedding the drug in rapidly dissolving layers of the hydrophilic polyvinyl caprolactame-polyvinyl acetate-polyethylene glycol polymer, , facilitated the rapid delivery of the hydrophobic drug cisplatin (CPT) to the epidermis when MNs were applied into the skin. CPT release profiles were assessed *in vitro* using Franz cells, while cisplatin *in vitro* cytotoxicity assessment was conducted to validate

the viability of A-431 epidermoid skin carcinoma (ESC) cells. To demonstrate the *in vivo* effectiveness of 3D printed MNs, we applied cisplatin loaded patches in BALB/c nude mice bearing epidermoid skin tumours.

MATERIALS AND METHODS

Materials

Cisplatin (CPT), retinoic acid (RTA) and rapamycin (RPC) were purchased from Sigma-Aldrich (Gillingham, UK), while Soluplus® (co-polymer of polyvinyl caprolactame-polyvinyl acetate-polyethylene glycol, MW=90,000-140,000 Da) was kindly donated by BASF (Ludwigshafen, Germany). A431 cells, a human squamous carcinoma cell line, was purchased from Cell Line Services (Eppelheim, Germany). Dulbecco‘s modified Eagle‘s medium (DMEM), thiazolyl blue tetrazolium bromide (MTT), L-glutamine, penicillin, streptomycin and heat inactivated foetal bovine serum (FBS) and trypsin were all purchased from Sigma-Aldrich, UK.

3D printing of microneedles

Cross-microneedle designs were developed using appropriate engineering software (SolidWorks by Dassault Systems), featuring cross-shaped cross-sections. The MNs were built by attachment to a solid 15x10x1.5 mm substrate, forming patches of 99 MNs each. The arrays were fabricated using a Form 2 SLA printer by Formlabs, with high resolution capabilities (25 and 140 microns for z and x axes, respectively). To obtain higher mechanical properties, the MN arrays, after being washed in isopropyl alcohol bath to remove excess resin, were cured under ultraviolet radiation for 60 minutes at 40 °C (MeccatroniCore BB Cure Dental station).

Inkjet printing of drug-loaded formulations on cross-MNs

The coating solutions were dispensed onto each cross-MN in the form of fine droplets using an inkjet printer (NanoPlotter 2.1, Gesim, Germany) with a piezo-driven dispenser (PicPip 300). The solutions were deposited through repeated coating cycles while MN arrays were positioned at 45° relative to the printing nozzle. For each coating cycle, 4 dots of a coating formulation were dispensed longitudinally to the axis of each MN and the process was repeated for 1-5 jetting cycles. Coating formulations were dispensed onto the 8 sides of the 4 fins of the cross-MNs by rotating the arrays 4 times. After 24 hr of incubation at room temperature, the solvent (de-ionised water) had evaporated, producing uniform and reproducible solid thin films on the MNs. The compositions of the coating formulations used are shown in Table 1 (Supplementary Data).

Scanning electron microscopy

The coated cross-MN arrays were mounted onto aluminium stubs using a double-sided carbon adhesive tape (Agar scientific, UK). Each coated cross-MN array was examined by SEM (Hitachi SU 8030, Japan) using a low accelerating voltage (0.6 kV). A low accelerating voltage was used to avoid electrical charges on the cross-MNs. The images of coated cross-MNs were captured digitally from a fixed working distance (11.6 mm) using different magnifications (30, 80, 110 or 120 x).

Optical coherence tomography (OCT)

OCT was used to assess the penetration depth and width of a single cross-MN into neonatal porcine skin. Neonatal porcine skin was excised from stillborn piglets (< 24 hr after birth)

and trimmed up to 500 µm using a dermatome (Integra Life SciencesTM, Padgett Instruments, NJ, USA). Skin of full thickness was stored at -20 °C and defrosted at room temperature when required. Two slices of skin (500 µm thick) were placed together in order to obtain samples with a thickness of 1000 µm and then used to prepare samples for OCT imaging. The stratum corneum was shaved to avoid hair follicle issues (the penetration of laser beam or imaging) using a regular razor blade. The double skin samples were secured on pre-prepared dental wax beds and covered with aluminium foil. Prototype moulded cross-MN arrays were fabricated for studying the penetration depth and width using poly(methylvinylether-co-maleic anhydride, PMVE/MA). MNs composed of 20% (w/w) PMVE/MA gel were prepared using laser-engineered silicone micromould templates. Briefly, silicone elastomer was poured into a custom-made aluminium mould and cured overnight at 40 °C. A laser-machine tool (BluLase® Micromachning System, Blueacre Technology, Dundalk, Ireland) with a laser (Coherent Avia, Coherent Inc., Pittsburgh, USA) λ = 355 nm and a pulse length of 30 ns (variable from 1 to 100 kHz) was then employed to produce MN moulds of specific height, width and interspacing, at the bases, of the MNs. A 20% (w/w) aqueous solution of PMVE/MA was prepared by adding the required mass of PMVE/MA to ice-cold deionised water, followed by vigorous stirring and heating at 95.0 °C until a clear gel was obtained, due to hydrolysis of the anhydride form of the copolymer to the corresponding acid. Upon cooling, the blend was then readjusted to a final concentration of 20% (w/w) by the addition of an appropriate amount of deionised water. This solution was then poured into the appropriate silicone micro-mould, centrifuged for 15.0 min at 3500 rpm and allowed to dry under ambient conditions for 24 hr. A total of 100 MN geometries were prepared for subsequent characterisation. Moulded MNs were transparent and prepared to replicate 3D printed MNs in order to facilitate OCT scans.

A 3D printed cross-MN array or the moulded prototype was applied for 30 s manually onto the skin using a fingertip. The penetration depths or widths of both types of MNs were measured by employing an OCT microscope (Michelson Diagnostics Ltd., Kent, UK). The skin was scanned at a rate of up to 15B-scans (2D cross-sectional scans) per second. All two-dimensional (2D) images were characterised using ImageJ® software (National Institute of Health, USA). The measurement scale was 1.0 pixel=4.2 µm which allowed precise investigations (both depth and width) of the cross-MNs created micro-conduits. False colour was applied to differentiate between the layer of stratum corneum and cross-MNs using Adobe Photoshop CS6® software (Adobe systems incorporated, USA). For the OCT evaluation, a total of 100 MNs were used in order to provide information about the actual penetration depths and widths obtained in the skin samples.

In vitro release studies of CPT coated MNs

Release studies of CPT in abdominal porcine skin were undertaken using Franz diffusion cells (PermeGear, Inc., PA, USA). Full thickness abdominal porcine skin was collected from a local slaughterhouse (Forge Farm Ltd, Kent, UK). The abdominal hair was shaved using a razor blade. The collected skin was stored at 4 °C until it was used. A total diffusion area of 1.1 cm^2 was used to assess the CPT release into the abdominal porcine skin. The skin (1000 µm thick) was cut for the permeability studies using a dermatome instrument (Padgett dermatome or blade, USA). Skin samples were then placed in phosphate buffered saline (PBS) (pH 7.4) for 1 hr before the *in vitro* studies. The cross-MN arrays were inserted into abdominal porcine skin (1000 µm) for 30 s using manual finger pressure. The pierced skin and cross MN array were mounted onto the donor compartment of a Franz diffusion cell. The temperature of the Franz cells was maintained at 37 °C using an automated water bath (Thermo Fisher Scientific, Newington, USA). Sample fractions (6-6.5 ml/hr) were collected

using an auto-sampler (FC 204 fraction collector, Gilson, USA) attached to the Franz diffusion cells. The quantitative analysis of CPT was undertaken using atomic absorption spectroscopy (Analyst 300, Perkin Elmer).

Atomic absorption spectroscopic analysis of CPT

The total platinum in CPT was determined using graphite furnace atomic absorption spectroscopy. A computer controlled atomic absorption spectrometer (Analyst 300, Perkin Elmer) equipped with a graphite furnace (HGA-800, Perkin Elmer) was used. The absorption was measured at a wavelength of 0.70 nm and 265.9 nm slit bandwidth. A deuterium lamp was used for continuous background correction in order to eliminate spectral interferences. Pyrolytic graphite coated tubes, without an integrated platform, were used and the atomization process was performed on the tube wall. High purity argon (99.99+ %) at a flow rate of 250 ml/min was used as a purge gas and its flow was interrupted during the atomization step. An aqueous platinum standard solution of 1000 mg/l Pt (Chem-Lab NV) was used. An intermediate solution of 5 mg/l Pt was prepared, using 0.2 % nitric acid as a diluent. Calibration standards (25-300 ppb) were prepared daily from the intermediate solution, using 0.2 % nitric acid as a diluent and stored in polyethylene containers. The final nitric acid concentration in the calibration standard solutions was 0.2% (w/v). The linear range was found to be between 0 and 300 ppb (µg/l). The furnace conditions during analysis are summarized in Table 2 (Supplementary Data). The reagent blanks (0.2% nitric acid) and calibration standards were measured in triplicate, whilst the platinum sample was evaluated in quadruplicate. A 10 µl aliquot of standard/sample was transferred on to the wall of the pyrolytic graphite coated tube using a high precision pipette. High purity water, obtained by distilling triply deionized water, was used throughout this study.

Visualization of cross-MN puncture in abdominal porcine skin

In order to study the efficiency of cross-MN arrays for the delivery of drugs in abdominal porcine skin, cross-MN arrays were used to deliver FlNa/SOL formulations into the skin. Skin penetration of FlNa was observed hourly (0-4 hr) using a fluorescent microscope (Nikon-ECLIPSE-90*i*, Japan) attached to a CCD camera (Nikon, Japan). Using the parafilm attached on an aluminium stub as a support, coated cross-MNs were pressed for 30 s (7 N pressure) in the dermatomed porcine skin (1000 µm) using a TA HD *plus* texture analyser (Stable micro system, Surry, UK). The parameters involved in the MN insertion process were: 1 mm/s pre-test, 0.2 mm/s test speed and 1 mm/s post-test speed. The skin samples were examined by fluorescent microscopy using an extended zoom (10 times) in order to visualise the upper skin surface. Additional experiments were conducted to study the piercing of the skin by methylene blue coated MNs for 0-24 hr, using a digital camera (Canon IXUS 130, UK). A Nanoplotter 2.1 was used to dispense 50 µl of methylene blue solution (20 mg methylene blue in 5 ml of distilled water) onto the MNs. Methylene blue coated MNs were allowed to dry for 24 hr at room temperature. Then each MN device was pressured onto the skin for 30 s (7 N application force) using a texture analyser. The methylene blue coating residues on the skin were recorded digitally, immediately after removal of the MNs from the samples of skin.

Penetration through porcine skin

The capability of the 3D printed MN arrays to effectively pierce porcine skin was investigated. A texture analyser (TA.HDplus, Stable Micro Systems) was employed to obtain the penetration force against displacement curves during piercing. Full thickness abdominal

porcine skin was procured from a local slaughterhouse (Forge Farm Ltd, Kent, UK). The MN arrays were fixed on the moving probe of the instrument using double-sided tape while the porcine skin was placed on waxed petri dishes which were attached to the fixed probe. The displacement rate of the moving probe was set to 0.01 mm/s, while force and displacement values were recorded throughout the experiment. Identical penetration tests through porcine skin were carried out using metallic MN arrays, as control experiments. All experiments were repeated 5 times.

Cytotoxicity tests

A-431 human skin epidermoid carcinoma cell line was cultured using DMEM culture medium (supplemented with 10% serum, 1% L-glutamine and 1% penicillin streptomycin) in an incubator maintained at 37 °C and 5% CO_2. The culture medium was changed every three days. The cytotoxicity of CRC, CPT and 5-FU (dissolved in either DMF, ethanol or deionised water, respectively) on A-431 human skin epidermoid carcinoma cell line was determined using a 3-[4, 5-dimethylthiazol-2-yl]-2, 5 diphenyl tetrazolium bromide (MTT) assay. Cells were seeded in a 24 well flat-bottom plate at a cell density of 1×10^6 cells/well and incubated for 24 hr. After 24 hr the cells were challenged with different concentrations of drugs as a function of incubation time. 100 μL of MTT solution (5 mg/ml) was added to each well at the end of the incubation time and incubated at 37 ºC for another 2 hr. The culture medium was discarded, followed by addition of 200 μl of acidified isopropanol to dissolve the MTT formazan crystals. 100 μl of the dissolved MTT formazan crystals were then transferred into a 96 well flat-bottom plate and the absorbance was read at 492 nm using a microplate reader. Non-treated cells were used as controls. Drugs were used at concentrations of 15, 25, 50, 100, 200, 400, 600 and 800 μg/ml.

Animal selection for in vivo MN testing

Nude albino hairless female mice (7–8 week; weighing 18–25 g) were selected for anti-cancer drug therapy *in vivo* trials. The strain of BALB/c nude mice used was CanN.Cg-foxn1^{nu}/CRL and they were developed from crosses and back-crosses between BALB/cABom-^{nu} and BALB/cAnNCrj-^{nu} strains of mice. The mice carried the inherited CanN.Cg-foxn1^{nu}/CRL gene and genetic monitoring confirmed them to be BALB/c nude mice. The animals were devoid of a thymus and incapable of producing T-cells and thus they were immunodeficient (Charles River 2014). Species, strain and gender selection were monitored and approved by Charles River UK Ltd.

Quantification and isolation of animal models

CanN.Cg-foxn1^{nu} (n=16, in total) mice were selected for *in vivo* anticancer therapy after subdividing into Group 1 (control), Group 2 (tumour-site treated with MNs), Group 3 (non-tumour-site treated MNs) and Group 4 (change in treatment site; tumour to non-tumour site). Group 2, 3, 4 (n=4) were counted as immunised using MNs while Group 1 (n=4) were used as controls (without drug). All mice were transferred to an isolator room at 7 weeks old. Female Balb/c mice were housed (<3 mice per cage) in solid bottom cages with litalabo 100% kiln dried spruce bedding and the mice were fed with a SDS VRF1 diet. Animals were identified by their ear clips.

Tumour development and cell inoculation

The tumour cell type, A431-human squamous carcinoma cell line (CLS, Eppelheim, Germany), was used to develop tumours in mice. The cells grew as monolayers in DMEM medium supplemented with 10 % (v/v) fetal bovine serum, 1% (v/v) L-glutamine and 0.5

(v/v) penicillin-streptomycin. Cells were cultured at 37 ^{o}C in a humid atmosphere of 5% CO_2. While variation in tumour development time and size was possible, typical palpable tumours developed within 6 days. Cells were inoculated at $1x10^6$ cells/dose/per mouse, subcutaneously in the flank of the animal, on day 0. As the experiments proceeded, body weight was measured daily, from day 0 (tumour cell inoculation) to 10 days. Tumour growth was monitored daily after cell inoculation, i.e. during tumour growth and throughout the drug treatment.

In vivo antitumor efficacy

An *in vivo* clinical study for the transdermal delivery of CPT in epidermoid skin carcinoma (ESC) A431 cell lines (skin cancer) using 3D printed cross-MN arrays was conducted. Cross-MN arrays were used to deliver CPT in female BALB/c nude mice. Once tumours reached >5 mm in diameter, the mice were anaesthetised by isoflorane inhalation and the groups were pierced with the MN patches (99 MN/array, 1.1 cm^2, height = 900 µm, width = 200 µm), with or without CPT (n=4 tumour-site application, n = 4 non-tumour-site application, n =4 change in treatment site, n=4 control). In vivo trials lasted for 10 days; however, the duration of the study depended on the response of the animal groups to the transdermal treatment of the ESC. Progressive disease is defined as an increase in relative tumour volume higher than 1.2-fold, stable disease as a relative volume between 0.7 and 1.2 of starting volume, partial response as measurable tumour with a reduction of more than 30 % (0 - 0.7) and complete response as the absence of any tumour.

The cross-MN arrays were coated to deliver 20 mg/kg CPT per dose for each animal. Coated MNs were inserted into the dorsal skin manually, using finger pressure for 30 s and then removed after 1 h (maximum application time to avoid animal discomfort). MNs were applied for 1 h due to the low amount of interstitial fluid in mice skin, which usually takes a

longer time to dissolve the coating material. The cross-MNs were pressed on the skin of the mice and secured using adhesive tape (3M, UK)to prevent any dislodgement.. Tumour volumes were determined by calliper measurements (Volume = D^3 x $\pi/6$). Results were expressed as relative tumour volume (rel. Vol_{tx} = Vol_{tx}/Vol_{t0}) and responses classified analogous to Response Evaluation Criteria in Solid Tumours (RECIST). The clinical protocol is depicted in Table 3 (Supplementary Data).

RESULTS AND DISCUSSION

3D printed MN patches using stereolithography

3D printed cross–MN arrays were fabricated by means of an additive manufacturing technique, stereolithography (SLA), which is used to build structures in a layer-by-layer manner from virtual CAD models. MNs consisted of a Class I biocompatible resin which was selectively cured using a light source, a UV laser, into hardened plastic patches via a photopolymerization process. The entire cross-linking process from liquid resin to highly polymerized solid structures during printing takes place in a few milliseconds while further curing under UV radiation was imposed, resulting in better mechanical properties of the printed MN patches.

As shown in Fig. 1a SLA was used to produce patches with 5 x 20 microneedles using a 800 μm spacing and a production rate of 10 min, rendering SLA an attractive and scalable approach for MN manufacturing. Cross-MNs were printed with approximately 900 μm height, 1000 μm width and consisted of four fins of 350 μm length each. The MN design allowed an increase in the amount of coated materials from a few micrograms to milligrams (up to 7.0 mg) compared to existing designs due to the increased surface. The interspacing distance varied form 0.4 – 1.0 mm in order to enhance drug delivery, reduce the

applied insertion force and negate the "bed of nail" effect [22]. Fig. 1a shows the built layers of the printed MNs, which are highly consistent and reproducible.

Inkjet printing was subsequently employed to apply coatings of cisplatin (CPT) and a hydrophilic polymer, polyvinyl caprolactam–polyvinyl acetate–polyethylene glycol (SOL), solutions using a piezoelectric dispenser. SOL is an amphiphilic polymer and it was selected due to its capacity to increase the solubility of water insoluble active substances and, hence, the dissolution rates [23-25]. By optimizing the applied voltage (mV) and the pulse duration (ms) of the piezoelectric nozzle we were able to produce droplets of 300 pL volume with a consistent particle size of 100 – 110 μm as observed by using the printer's stroboscope. In addition, the nozzle tip was kept in close proximity to the MN surface to avoid any material losses or deposition on the MN substrate. This is evident in Fig. 1b which shows SEM images of high precision and reproducible cross-MN coatings without any satellite droplets. The piezoelectric nozzle achieved uniform coatings avoiding the formation of bulky layers that affect the MN piercing capacity and dissolution of the coated material.

Printability and scale – up

3D printing is a technology that permits the fabrication of structures that feature degrees of complexity that are unattainable via conventional manufacturing methods. However, regarding applications that require great accuracy and detail at the microscale, typical 3D printing systems in the low-cost range pose restrictions in terms of resolution. SLA commercial printers have a maximum resolution capability that is determined by the size of the focal point of the laser (for the branch technology of SLA, Digital Image Processing-DLP, the maximum resolution corresponds to the minimum size of the volumetric pixel that the projector can flash) as well as by the laser and platform movement minimal step in the x, y and z axes [25].

It is therefore evident, that the printer itself sets a minimum regarding the MN tip dimensions which may be out of the geometrical range that guarantees effective and pain-free penetration through the skin. In this work, MN arrays featuring tips of 100 μm were successfully and reproducibly manufactured and their penetration capability through porcine skin under small drug loads was confirmed.

The reproducibility and quality of the MNs was improved when printing-in-an-angle was implemented. This is because the quality of SLA printed parts is influenced by the cross-sectional area in the z-axis. During the printing of each layer, the z-axis cross-sectional area is attached onto the silicon cover of the resin tank and peeled off by a wiper, a process that can create distortions to the printed part. Minimising this area (building the MN patches in an angle) will also minimise the developed stresses during the peel-off process, yielding better end-part quality. It is noteworthy that although part anisotropy is a well-established fact about 3D printing when layers are printed in an angle, SLA parts are considered mechanically isotropic, which guarantees that the mechanical parameters of the arrays are not affected by the angle of printing [26].

On the other hand, an important set of parameters that can alter the mechanical properties of the arrays is the post-process curing settings. The time and temperature of curing under UV light straightforwardly affects the mechanical properties of the material and additional research is required to assess this effect. It is however proved in this work that all MNs penetrated the skin effectively with no needle failure observed, meaning that the curing parameters that were specifically used yielded MNs with sufficient mechanical strength and stiffness.

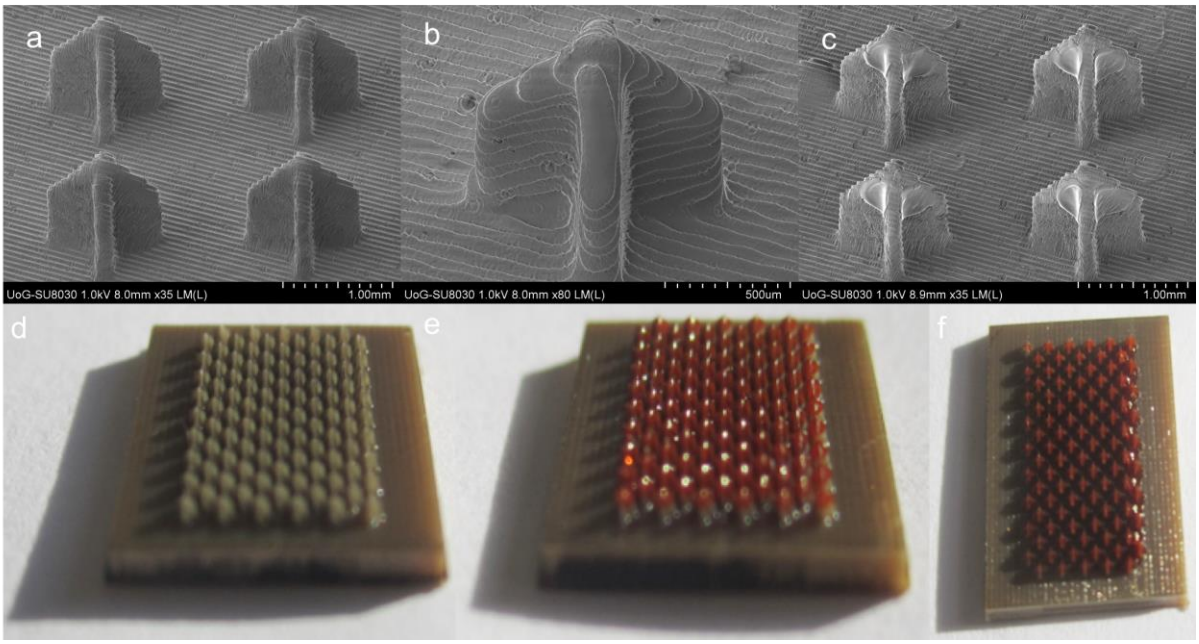

Fig. 1: SEM images of uncoated (A1-2) and coated (A3) 3D printed cross-MNs at various magnifications, where the photopolymerised layers can be clearly seen. Optical images of uncoated (B1) and coated (B2-3, red dye) 3D printed cross – MN patches. 3D printed cross-MN patches of 5 x 20 needles were fabricated and subsequently coated with placebo or active formulations. The MN patches were coated with a red dye using inkjet printing in order to apply 8 micro-droplets on each MN fin to achieve high loadings.

Currently there are no commercial MN products due to technical limitations as discussed previously such as limited drug loading, dose consistency and scalability issues. Polymeric MNs are fabricated using moulding and dip – coating approaches which renders large-scale manufacturing impractical. In contrast, the upscaling of SLA fabricated MNs depends solely on the introduction of large volume printers or the in – line use of the existing printers. 3D printed MNs using SLA are expected to open new horizons for drug delivery purposes due to the low cost of the printers and printing materials and rapid fabrication times.

Optical coherence tomographic (OCT) studies

OCT was utilized for assessing skin penetration of 3D printed and moulded prototype cross-MNs into porcine skin [27]. OCT provides a broad spectrum of information on skin penetration of MNs using a laser technology that can monitor, in real time, the penetration of drug coated MNs into deep skin tissue. As shown in Fig. 2, 3D printed MN prototypes produced a set of uniform and reproducible holes in the skin, using a manual application force. Prior to skin piercing, the OCT instrument was calibrated by using parafilm of 8 compact layers (approx. 1000 µm thickness) [28]. Though the application force was finger pressed, moulded cross-MNs penetrated to a skin depth of up to 154.1(±18.0) µm (Table 1). This experiment was necessary to provide an accurate estimation of the penetration pattern in the parafilm samples. As shown in Fig 2 3D printed cross-MNs showed a penetration depth of more than 80% of their length in neonatal porcine skin. The penetration efficiency of the cross-MNs was attributed to different factors such as the soft neonatal porcine skin, which was easy to pierce, but also to the cross-MN design which plays a significant role in the efficient tearing of the skin and the creation of micro-channels.

The data in Table 1 show a comparison of the penetration characteristics of different skin layers (both the parafilm mimic and real porcine skin). Interestingly, it was found that both the penetration depth and width of 3D printed cross-MNs demonstrated that they have better piercing capacity compared to the moulded prototypes.

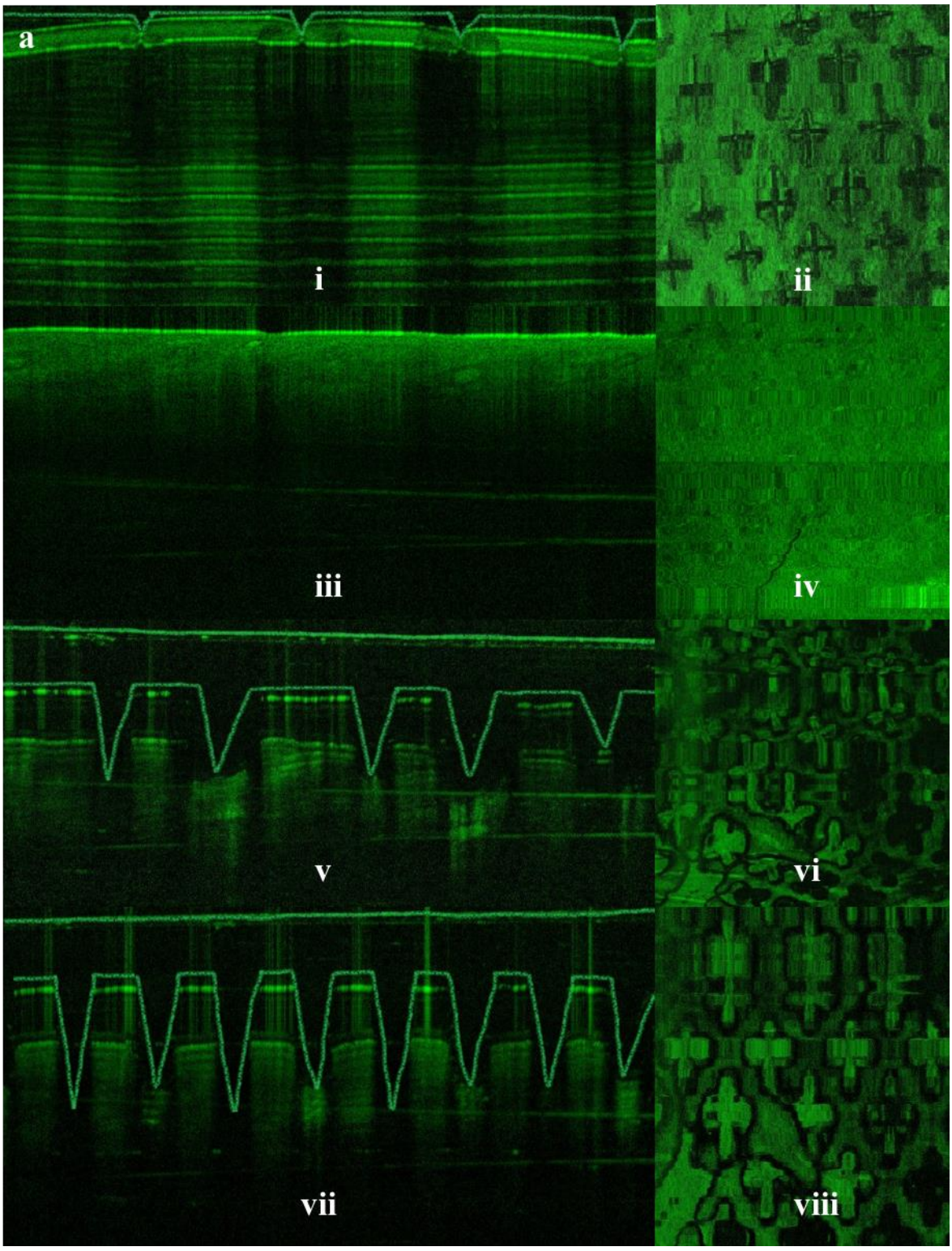

Fig. 2: False colour 2D still images of cross-MNs showing the real-time penetration into the neonatal porcine skin using OCT. i) Control test with parafilm, iii) blank skin before experiment, v) insertion of cross-MNs, vii) insertion of prototype MNs, ii), iv), vi) and viii) are re-sliced or top view images of i, iii, v and vi, respectively (scale bar 100 µm).

Table 1: Comparison of penetration characteristics (depth and width) in parafilm and porcine skin using manual finger pressure.

Experiment Design	Penetration depth (µm) (Mean±SD), n=5	Penetration depth (%)	Penetration width (µm) (Mean±SD), n=5	Penetration width in percentage (%)
Control (in parafilm)	227.1±18.0	25.0%	80.4±24.7	20.1%
3D cross-MNs (in skin)	737.7±63.7	82.0%	225.5±55.3	56.4%
Moulded cross MNs (in skin)	660.2±68.5	73.4%	215.5±31.5	53.9%

Visualization of cross-MN puncture into abdominal pig skin

For the delivery of active substances via cross-MNs it was important to demonstrate that they penetrate the *stratum corneum* efficiently. Thus, initial visualization studies were undertaken by using FlNa/SOL coated formulations on cross-MNs. Fluorescent microscopic images, Fig. 3a, demonstrated real time visualization of FlNa/SOL formulations at different time intervals (0-4 hr) into the skin. It can be clearly seen that FlNa is deposited into the skin and that by applying a 3 N force, cross-MNs could successfully penetrate the stratum corneum and deliver the dye into the skin. As shown in a similar study [28], the removal of polymeric MNs resulted in perforations in the stratum corneum and subsequent deposition of the Nile blue dye in the epidermis.

The optical visualization of cross-MNs coated with methylene blue, and attached on adhesive tape, is shown in Fig 3c-d. The results confirm that the cross-MNs can successfully puncture the skin and penetrate the *stratum corneum* without necessarily applying excessive forces. It is clear from the data in Figure 5 that the skin puncture formed an identical pattern corresponding to the arrangement of the cross-MN patches. Both studies showed a rapid close of the MN induced micro – pores within 4-6 h without leaving any visual marks on the skin.

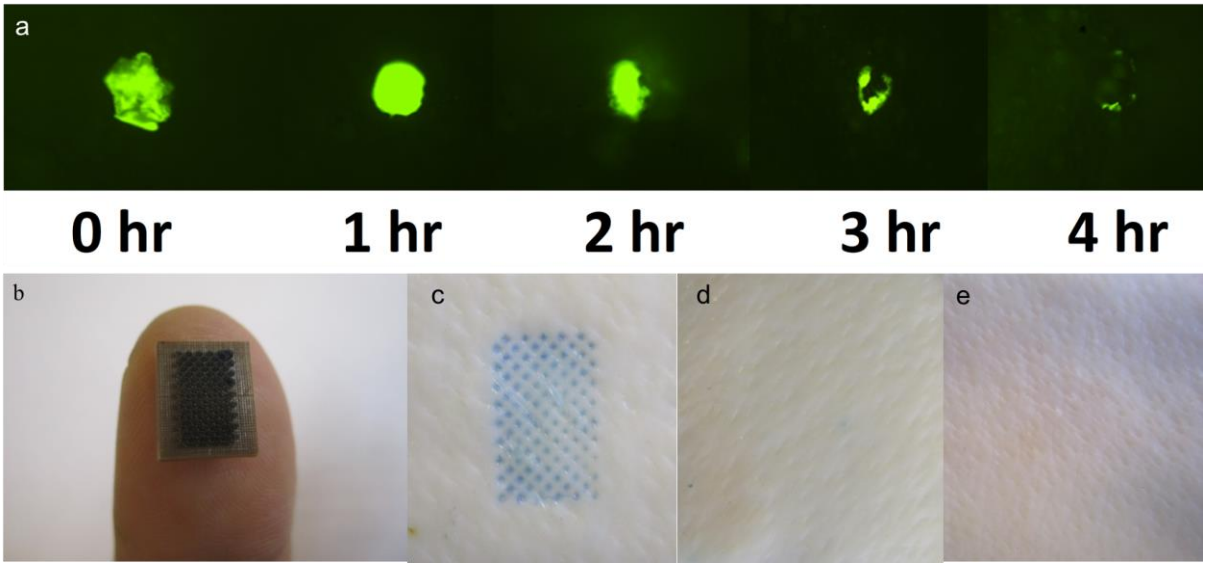

Fig. 3: a) Representative *in vitro* fluorescent images for FlNa/SOL formulations delivered into abdominal porcine skin at 0-4 hr time intervals (coated cross-MNs were pressed for 30 s in porcine skin (1000 µm) using a TA HD plus texture analyser) and digital camera photographs taken during cross-MN puncture experiments with (a) cross-MN patch system, (b) immediately after application, (c) observation of skin after 6 hr and (d) skin after 24 hr.

Penetration through porcine skin

3D printed polymeric cross-shaped and metallic MN arrays were tested for their penetration capability through porcine skin, using a texture analyser. All the experiments were successful in terms of needle penetration and no broken or damaged MN were detected after the

experiments. The penetration force against displacement curves were obtained for both MN groups and representative data are displayed in Fig. 4a.

As illustrated, the obtained experimental curves featured an initial linear segment, with almost equal slopes for the two MN groups. Considering the mechanical behaviour of the skin which is considered elastic within this load range [29], a linear force to displacement relationship should be anticipated prior to insertion. Nonetheless, the slope of the curve is constantly changing, indicating that the insertion process is a combination of early, gradual penetration until the highest force is reached, in agreement with findings that have been documented elsewhere [30]. Evidently, after a maximum was reached, the force dropped dramatically, specifying the point of full needle insertion. A comparison between the two groups reveals that the maximum penetration force required for the 3D printed cross MN is significantly lower than the one required for the metallic ones (Fig. 1, Supplementary Data).

In vitro release of cisplatin

Initially, a thorough investigation on inkjet printing of active coatings was conducted by applying CPT/SOL layers on 3D MNs. As shown in Table 4 (Supplementary Data) by altering the number of inkjet cycles a range of CPT/SOL (1:1 wt/wt) amounts were applied on the MN surfaces. The CPT release studies were carried out to determine the coatings with the fastest *in vitro* drug release performance. Due to UK Home Office restrictions, MNs can only be applied for 1 hr during *in vivo* trials and thus CPT release should take place within the same time frame. The total coated material varied from 0.3–1.6 mg, while CPT loading varied from 150-770 μg.

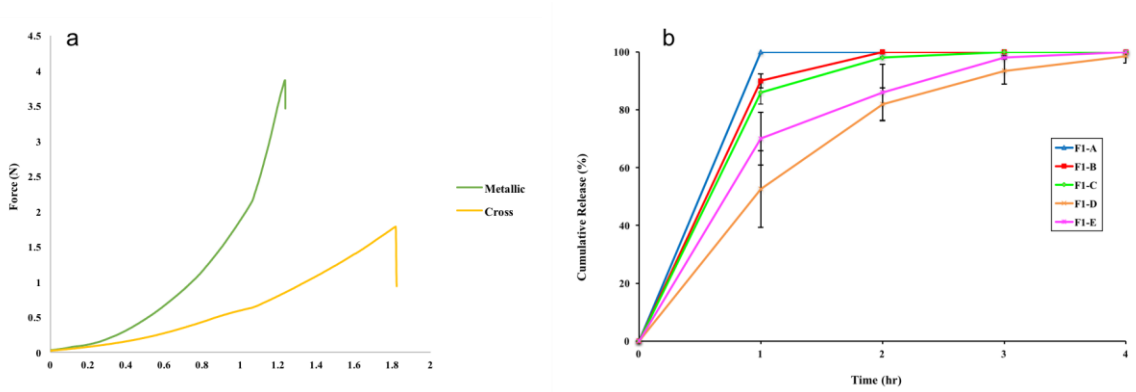

Fig. 4: *a)* Comparison of penetration force versus displacement for metallic and 3D printed MNs, *b)* In vitro Franz cell release studies**.** Release of CPT/SOL coated formulations into 1000 µm of skin for 4 hr (mean ± SD, n=3). Inkjet coated formulations of various CPT loadings were designed to facilitate rapid drug release within 1 h.

Subsequently, Franz cells studies were conducted to evaluate the release of CPT from the coated formulations. Most of the CPT was found in the receptor compartment and negligible amounts were detected in the skin after 4 hr. It is evident, Fig. 4b, that approximately 100% of CPT was released from the cross-MNs even at very high drug loadings. The Franz cell studies revealed that CPT release was dependent on the amount of drug loaded onto the MNs. For low CPT loadings a rapid release occurred, with 90-100% of CPT being released within the first hour (F1-F3). The fast release rates are related to the thin CPT/SOL layers applied by inkjet processing and the solubilizing efficiency of SOL. At higher loadings (F4-F5) slower release rates were observed varying from 45-65% and 95-100% after 1hr and 4 hr, respectively. The slow release rates were attributed to the higher loading amounts on the MN surfaces and the low water solubility of CPT. Based on the foregoing findings F1 was selected as the most suitable formulation to bring forward for the animal studies.

In vivo clinical trial of CPT loaded cross-MNs

Tumours developed on Balb/c nude mice within 1 week, after subcutaneous injection of A431-human squamous carcinoma cells. As stated in the clinical protocol, four groups were treated with unloaded and drug coated cross-MNs. In order to avoid the MNs being dislodged and any discomfort to the mice, the MNs were placed on a specifically designed frame, pierced on the mice and fastened with adhesive tape (Fig. 2, Supplementary Data).

Fig. 5 illustrates images of the four groups used for the cross-MN treatment over a period of 10 days, with the control group (A1, uncoated MNs), and MN piercing applied on the tumour site (B1, CPT coated) presented. For the other two groups, MNs were applied in close proximity to the site of the tumour (C1, CPT coated) and for the group wherein treatment was changed on day eight (D1, CPT coated), the piercing of cross-MNs was moved from the tumour site to a flat surface of the body of the animals.

The treatments with cross-MNs were well tolerated by the mice and no evident signs of toxicity or weight loss were observed. Only a slight increase in weight (Fig. 3, Supplementary Data) was found for the control and the tumour-site treated animal groups. As expected, the control treatment with uncoated cross-MNs led to tumour progression and the animals did not survive. These animals were euthanized at the end of the treatment period due to the increased tumour growth. Interestingly, the treatment with cross-MN piercing on the tumour site was partial and led to a slight regression in the tumours compared to the control group. This is obvious from the findings shown in Fig. 6a where the tumour-site treatment led to only a 30% regression. It is not well understood why this type of treatment did not present the expected results. It was attributed to the dislodgment of MNs or the inappropriate piercing of cross-MNs due to the tumour shape where only a small number of individual MNs punctured the tumour leading to the delivery of small amounts of CPT. Indeed, small traces of coated material were found after the use of MNs.

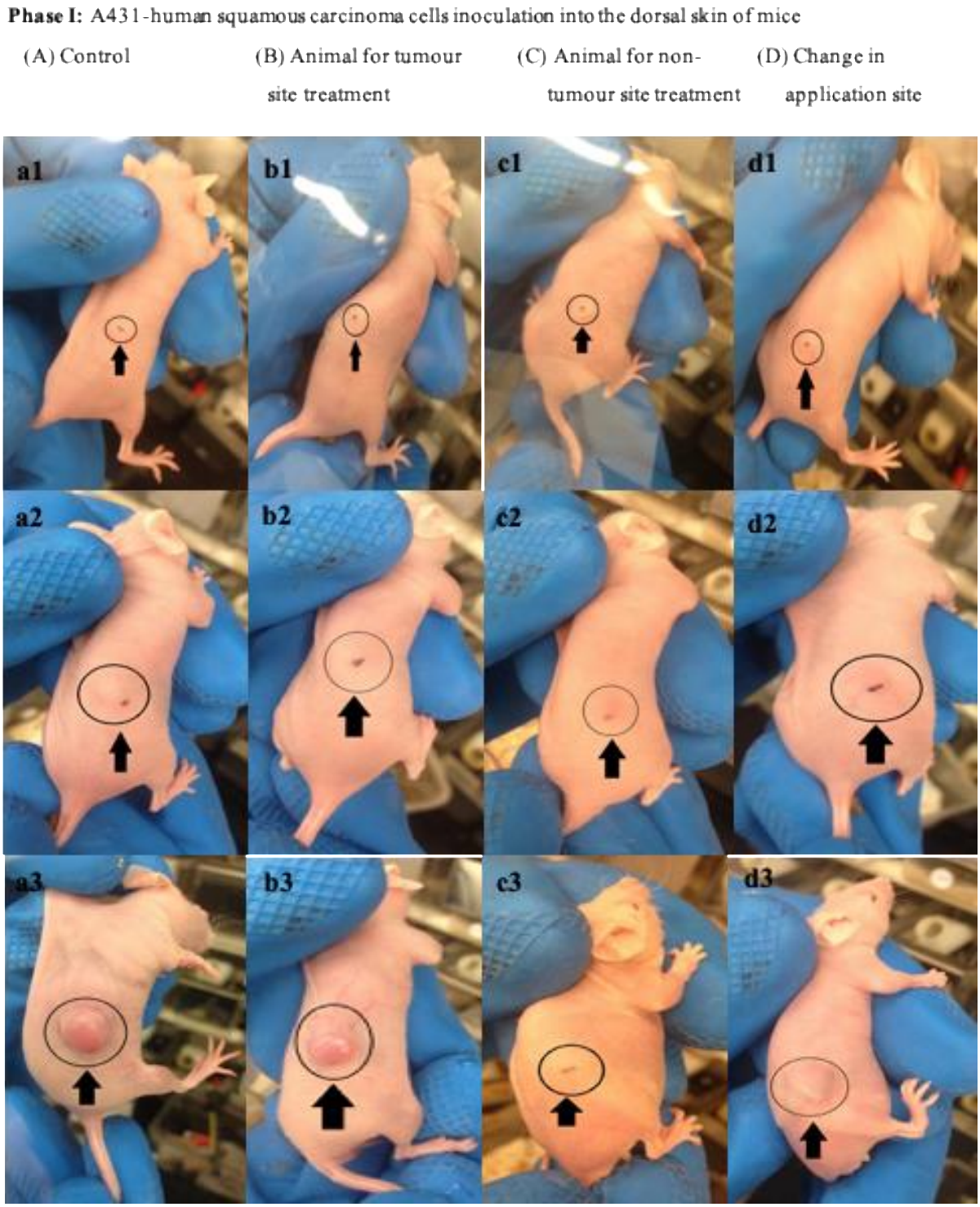

Fig. 5: In vivo evaluation of 3D printed cross–MNs loaded with CPT in Balb/c nude mice. Digital photographs of cross-MN treated animal skin; (a1, a2, a3) treatment of animal without CPT, (b1, b2, b3) CPT loaded MNs treatment upon tumour site, (c, c2, c3) CPT

loaded MN treatment at non-tumour site and (d1, d2, d3) changes in treatment site after 8 days.

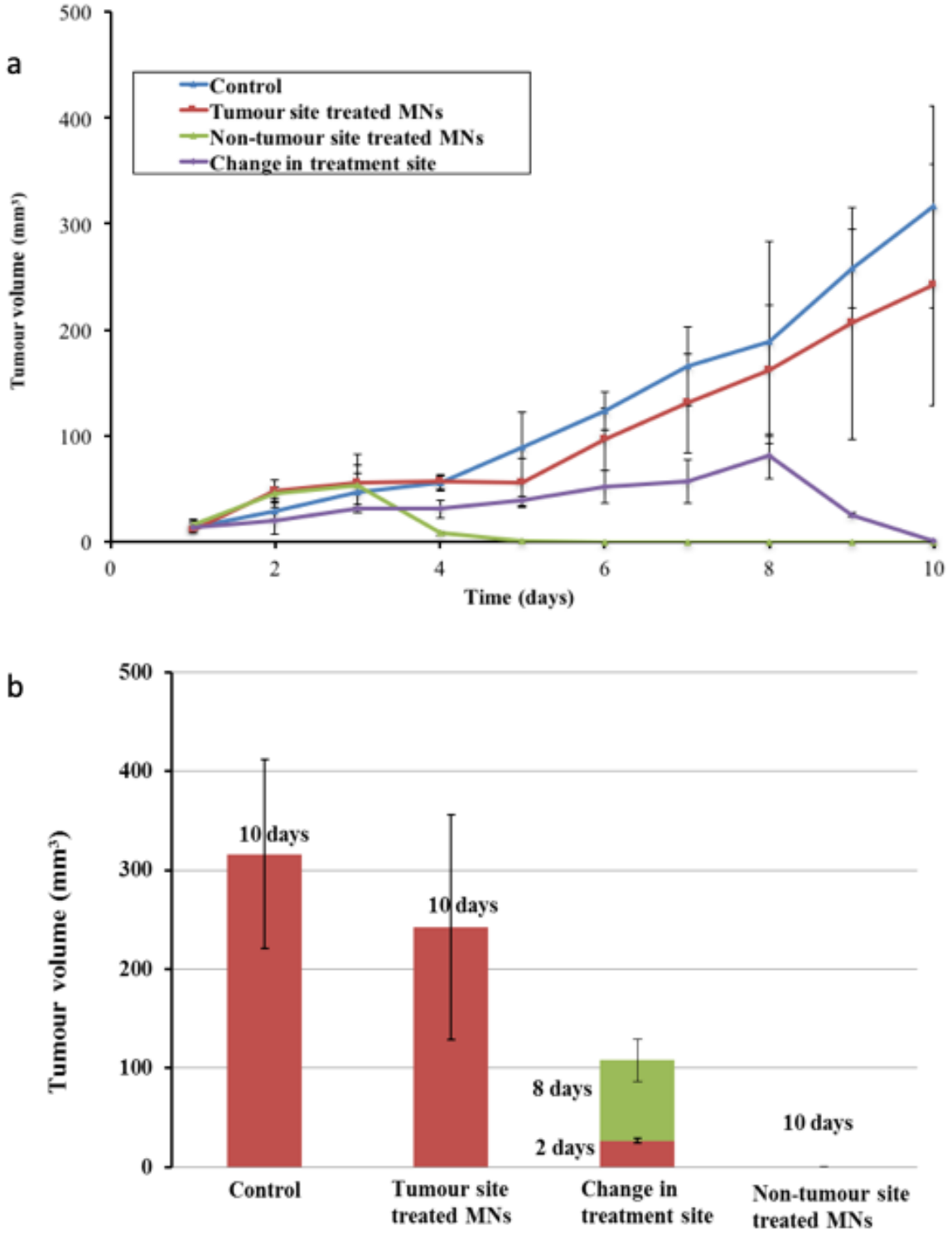

Fig. 5: In vivo evaluation of 3D printed cross–MNs loaded with CPT in Balb/c nude mice. a) Tumour volume (mm^3) regression after treating with CPT loaded cross-MNs, b)

Comparative tumour volume (mm^3) regression for 10 days after treatment with CPT loaded cross-MNs.

This is not unheard of and it has been previously observed that skin hampers drug permeability when MNs are applied with poor contact to the affected site [31]. Another possible reason could be the presence of small amounts of interstitial fluid in the tumour site, which will require a longer application time to dissolve the coating materials into the skin. It is possible that the administration of MNs created a depot at the administered tumour site and CPT release occurred slowly to the site of action [32]..

The treatment with CPT loaded cross-MNs applied on a non-tumour site showed a remarkable anti-cancer effect and complete tumour regression. As shown in Fig. 6a, the effect occurred in 24 hr and resulted in the survival of the mice being extended. The treatment was applied three days after the tumour reached a critical volume (5 mm^3) and a regression from 8.2 mm^3 to 1.3 mm^3 was recorded. This cancer trace was totally eliminated on the fifth day with 100% animal survival rates. The tumours disappeared and did not re-grow for the duration of the trials. This treatment corresponds to a major improvement in the therapeutic efficacy of CPT loaded MNs for the treatment of A-431 induced squamous carcinoma.

The data in Fig. 6a shows 100% tumour regression in comparison to the control group. The rapid response to the CPT treatment of this group is a strong indication of the successful release of the drug within the skin tissue of the mice. We assumed that CPT was released faster compared to the *in vitro* Franz cell experiments since the skin of the mice (both epidermis and dermis) is far less thick when compared to that of abdominal porcine skin, so deeper penetration depth can be achieved. Perhaps more importantly, the drug only has to cross the epidermis for *in vivo* delivery (as blood circulation is under the epidermis)

whereas *in vitro,* it has to cross the entire length of skin to be detected in the receptor chamber [33].

Furthermore, due to the application of MNs on non-tumour sites the drug must have been delivered systemically and destroyed the tumour by reaching it through the circulation. In this investigation, CPT release studies were carried out employing 900 µm of excised abdominal porcine skin. However, total skin thickness of mice (approximately 500-600 µm) enhanced the permeation of CPT across the skin.

In addition, noticable results were also achieved when the CPT administration was switched from the tumour site to the neighbouring mice tissue (flat) where rapid tumour eradication took place within two days. As mentioned in the protocol, the treatment change was scheduled for day 8 and by that time, tumour growth (161.4 mm^3) was highly progressive. Nevertheless, a significant reduction of 93% (Fig. 6b) was attained within the last two days of the treatment. The theraputic improvement from large volume tumours strongly demonstrates the efficient delivery capacity of cross-MNs for systemic administration of CPT via transdermal application.

Histopathological studies

The histological characteristics of haematoxylin and eosin stained sections of the tumour/skin samples of A431 squamous cell carcinoma inoculated BALB/c mice were examined for both control and CPT loaded microneedles. The control mice group treated with unloaded MNs showed uncontrolled proliferation of cancer cells. In the data shown in Fig. 6a-c, major histological changes were observed in skin tissue. The control group, where the growth of tumour cells was rapid in nature, formed a necrotic core (due to the lack of blood supply) and ulcerative surface in the centre. A similar phenomenon can be observed in

Fig. 6b, where tumours are only displaying their necrotic core, without showing an ulcerative surface [34].

However, in Fig. 6 (d, e), the MNs piercing the tumour site demonstrated some histopathological changes such as the formation of a thin fibrous capsule and varying degrees of an encircling inflammatory reaction. The tumours were also showing a rapid growth with a high mitotic index. The results are not consistent as the tumour-site MNs are difficult to fully penetrate due to the uneven surface of the tumour site. This resulted in poor contact with the dorsal skin of the mice, especially in cases where the mice moved often and sporadically around the cage, as their movement heightens the chance of the MNs coming loose. This is in agreement with a previous study which suggested that poor contact to mice skin may dislodge the MN device before drug release [31]. This phenomenon was attributed to the irregular shape of the skin tumour on the mice skin. Finally, as shown in Fig. 6 (f, g) the non-tumour-site MNs (n = 3) demonstrated significant control of cancer cells by suppressing A-431 human squamous carcinoma cells. The tumour appeared small, while the majority of skin tissue shows chronic active inflammation and oedema in the subcutis.

Analysis of the above results has made it evident that 3D printed MNs can effectively penetrate the superficial epidermis and thus might reduce the risk of skin damage without pain sensation. However, the skin tumours might have a complex tropism to human cells due to the differences between cell lines, xenografts and *in vivo* situation. Complex interactions between transformed cells and the surrounding tumour environment consisting of extracellular matrix molecules, stroma cells, parenchymal cells and immune cells are not represented in such xenograft approaches [35]. The histopathological changes in the tumour/skin cancer cells also support the comparative tumour volume (mm^3) regression after 10 days, which were seen in cross-MNs mediated CPT treated inoculated mice.

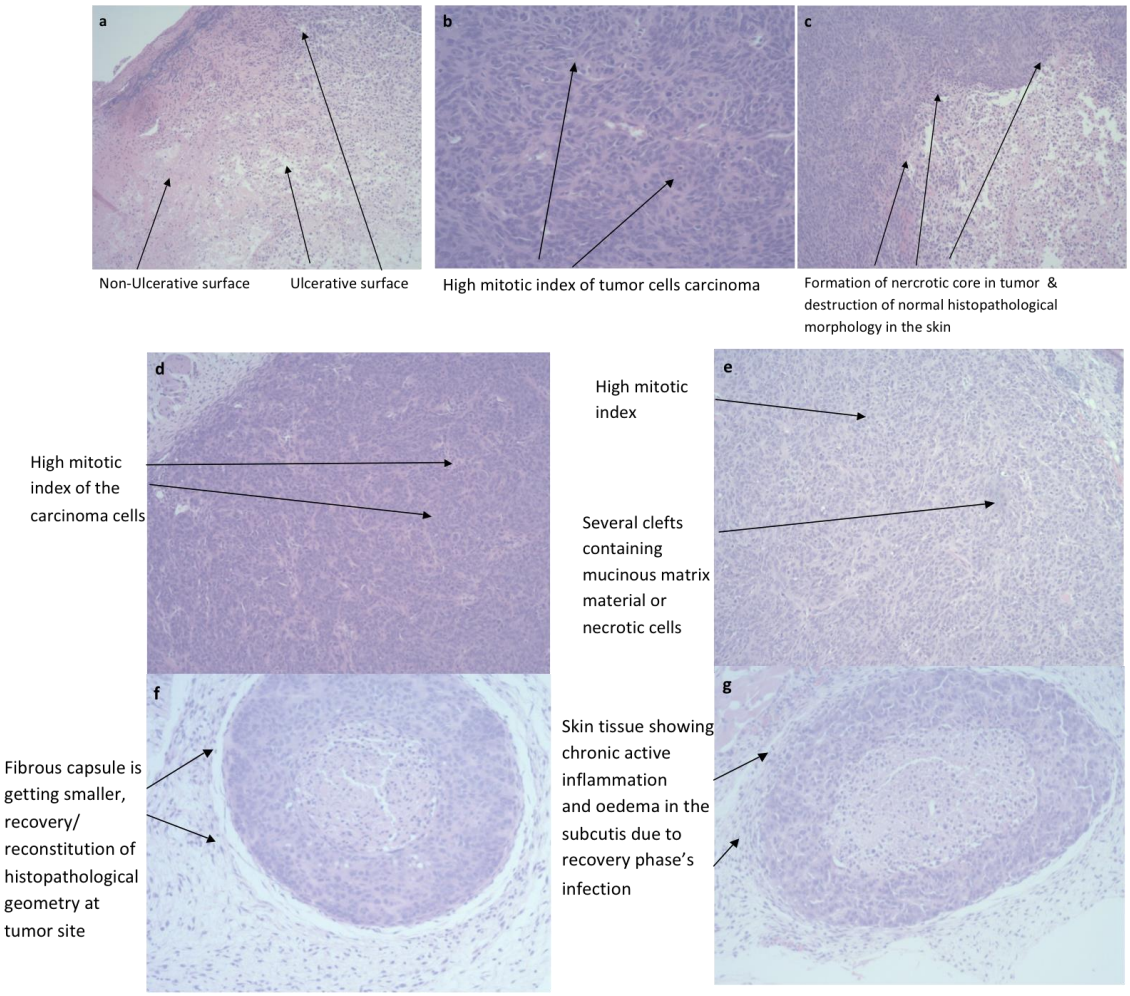

Fig. 6: Transverse section of skin of BALB/c mice stained with hematoxylin and eosin stains. Control (a – c) magnification x100); (b) control (magnification x200). (a and b) Inoculated mice treated on tumour site and (c and d) inoculated mice treated on non-tumour site with CPT loaded 3D printed MNs (magnification x100).

Also, histopathological changes in MN mediated CPT delivery permit normal skin reformation without skin damage. In summary, it was confirmed that non-tumour-site treatment for anticancer therapy using MNs is more effective (systemic effect) in eliminating A431 squamous carcinoma cells than a tumour-site treated microneedles group.

CONCLUSIONS

In this study we introduced, for the first time, a novel 3D printed MN design fabricated using a biocompatible polymer for cancer treatment. This novel MN design can be loaded with different amounts of formulation varying from a few micrograms to milligrams in a single cross-MN array. The design of the MNs is expected to open new horizons for the transdermal delivery of various drugs, where skin is the prefered delivery route. The combination of stereolithographic 3D printing and inkjet coating of MNs generates accurate and reproducible MN arrays and excellent coatings with desirable drug amounts and no material lossess, and can be easily scaled-up. We also demonstrated, again for the first time, 3D printed MN mediated CPT delivery for cancer treatment to A431-human squamous carcinoma zenografts. The cancer treatment via CPT loaded cross-MNs led to complete tumour suppresion and elimination with 100% animal survival.

AUTHOR INFORMATION

Corresponding Author

* Corresponding Authors: Prof. D. Douroumis, E-mail: d.douroumis@gre.ac.uk, Tel: +44 (0) 2083 31 8440.

Author Contributions

The manuscript was written through contributions of all authors. All authors have given approval to the final version of the manuscript.

Notes

The authors declare no competing financial interest

ACKNOWLEDGMENTS

This study was supported in part by Wellcome Trust grant number: WT094085MA "Optical coherence tomographic characterisation of drug delivery systems and biomaterials".

REFERENCES

[1] Moreno, E.; Schwartz, J.; Calvo, A.; Blanco, L.; Larrea, E.; Irache, J.M.; Sanmartín, C.; Coulman, S.S.; Soto, M.; Birchall, J.C.; Espuelas, S. Skin vaccination using microneedles coated with a plasmid DNA cocktail encoding nucleosomal histones of Leishmania. *Int. J. Pharm*. 2017, 533, 236-244.

[2] Sanjay, S.T.; Dou, M.; Tavakoli, H.; Ma, L.; Xu, F.; Li, X. Recent advances of controlled drug delivery using microfluidic platforms. *Adv. Drug Deliv. Rev*. 2018, 128, 3-28.

[3] Prausnitz, M.R.; Mitragotri, S.; Langer, R. Current status and future potential of transdermal drug delivery. *Nat. Rev. Drug Discov*. 2004, 3, 115–124.

[4] Leone, M.; Mönkäre, J.; Bouwstra, J.A.; Kersten G. Dissolving Microneedle Patches for Dermal Vaccination. *Pharm. Res*. 2017, 34, 2223-2240.

[5] Kim, Y.C.; Park, J.H.; Prausnitz M.R. Microneedles for drug and vaccine delivery. *Adv. Drug Deliv Rev*. 2012, 64(14), 1547-68.

[6] Lahiji, S.F.; Dangol, M.; Jung, H. A patchless dissolving microneedle delivery system enabling rapid and efficient transdermal drug delivery. *Sci. Rep*. 2015, 5, 7914.

[7] Ita, K. Transdermal Delivery of Drugs with Microneedles—Potential and Challenges. *Pharmaceutics* 2015, 7, 90-105.

[8] Jain, A.K.; Lee, G.H.; Gill, H.S. 5-Aminolevulinic acid coated microneedles for photodynamic therapy of skin tumors. *J. Control. Release* 2016, 10, 72-81.

[9] Hao, Y.; Dong, M.; Zhang, T.; Peng, J.; Jia, Y.; Cao, Y.; Qian, Z. Novel approach of using Near-Infrared Responsive PEGylated gold nanorod coated poly(l-lactide) microneedles to enhance the antitumor efficiency of Docetaxel-loaded MPEG-PDLLA micelles for treating an A431 tumor. *ACS Appl. Mater. Interfaces* 2017, 9, 15317-15327.

[10] DeMuth P.C.; Min, Y.; Huang, B.; Kramer, J.A.; Miller, A.D.; Barouch, D.H.; Hammond, P.T.; Irvine, D.J. Polymer multilayer tattooing for enhanced DNA vaccination. *Nat. Mater*. 2013, 12, 367-76.

[11] Ali, A.A.; McCrudden, C.M.; McCaffrey, J.; McBride, J.W.; Cole, G.; Dunne, N.J; Robson, T.; Kissenpfennig, A.; Donnelly, R.F.; McCarthy H.O. DNA vaccination for cervical cancer; a novel technology platform of RALA mediated gene delivery via polymeric microneedles. *Nanomedicine* 2017, 13(3), 921-932.

[12] Chiappini, C.; Martinez, J.O.; De Rosa, E.; Almeida, C.S.; Tasciotti, E.; Stevens, M.M. Biodegradable nanoneedles for localized delivery of nanoparticles in vivo: exploring the biointerface. *ACS Nano*. 2015, 9(5), 5500-5509.

[13] Kodama, H.J. A Scheme for Three-Dimensional Display by Automatic Fabrication of Three-Dimensional Model. *IEICE* 1981, 64, 237.

[14] Hull, C.W. Apparatus for production of three-dimensional objects by stereolithography. US4575330 (1986).

[15] Voet, V.S.D.; Strating, T.; Schnelting, G.H.M.; Dijkstra, P.; Tietema, JM.; Xu, J.; Woortman, A.J.J.; Loos, K.; Jager, J.; Folkersma, R. Biobased Acrylate Photocurable Resin Formulation for Stereolithography 3D Printing. *ACS Omega* 2018, 3 (2), 1403–1408

[16] Palaganas, N.B.; Dacula Mangadlao, J.D.; de Leon, A.C.C.; Palaganas, J.O.; Pangilinan, K.D.; Lee, Y.L.; Advincula, R.C. 3D Printing of Photocurable Cellulose Nanocrystal Composite for Fabrication of Complex Architectures via Stereolithography. *ACS Appl. Mater. Interfaces* 2017, 9 (39), 34314–34324

[17] Thrasher, C.J.; Schwartz, J.J.; Boydston, A.J. Modular Elastomer Photoresins for Digital Light Processing Additive Manufacturing. *ACS Appl. Mater. Interfaces* 2017, 9 (45), 39708–39716

[18] Economidou, S.N.; Lamprou, D.A.; Douroumis, D. 3D printing applications for transdermal drug delivery, Int. J. Pharm. 2018, 544, 415-424.

[19] Gittard, S.D.; Miller, P.R.; Chunming, J.; Martin, T.N.; Boehm, R.D.; Chisholm, B.J.; Stafslien S.J., Daniels, J.W.; Colz, N.; Monteiro-Riviere, N.A.; Nasir, A.; Narayan, RJ. Deposition of Antimicrobial Coatings on Microstereolithography-Fabricated Microneedles. *JOM* 2011, 63, 59-68.

[20] Lu, Y.; Mantha, S.N.; Crowder, D.C.; Chinchilla, S.; Shah, K.N.; Y.H. Yun, R.B. Wicker, J. Choi. Microstereolithography and characterization of poly(propylene fumarate)-based drug-loaded microneedle arrays. *Biofabrication* 2015, 7(4), 045001.

[21] Shain, A.H.; Bastian, B.C. From melanocytes to melanomas. *Nat. Rev. Cancer*. 2016, 16, 345-358.

[22] O. Olatunji, O.; Das D.B.; Garland, M.J.; Belaid, L.; Donnelly, R.F. Influence of array interspacing on the force required for successful microneedle skin penetration: theoretical and practical approaches. *Pharm. Res.* 2015, 27, 2213-2220.

[23] Uddin, J.; Scoutaris, N.; Klepetsanis, P.; Prausnitz, M.; Chowdhry., B.Z.; Douroumis, D. Inkjet printing of transdermal microneedles for the delivery of anticancer agents. *Int. J. Pharm.* 2015, 494, 593-602.

[24] Ross, S.; Scoutaris, N.; Lamprou, D.; Mallinson, D.; Douroumis, D. Inkjet printing of insulin microneedles for transdermal delivery. *Drug Deliv Transl Res*. 2015, 5, 451-61.

[25] Pere, C.P.P.; Economidou, S.N.; Lall, G.; Ziraud, C.; Boateng, J.S.; Alexander, B.D.; Lamprou, D.A.; Douroumis D. 3D printed microneedles for insulin skin delivery. *Int J Pharm.* 2018, 544, 425-432.

[26] Dizon, J.R.C.; Espera, A.H.; Chen, Q.; Advincula, R.C. Mechanical characterization of 3D-printed polymers. *Addit. Manuf.* 2018, 20, 44–67.

[27] Donnelly, R.F.; Garland, M.J., Morrow, D.I.J.; Migalska, K.; Raghu Raj Singh, T.; Majithiya, R.; Woolfson, A.D. Optical coherence tomography is a valuable tool in the study of the effects of microneedle geometry on skin penetration characteristics and in-skin dissolution. *J. Control. Release*. 2010, 147, 333-341.

[28] Larrañeta, E.; Moore, J.; Vicente-Pérez, E.M.; González-Vázquez, P.; Lutton, R.; Woolfson, A.D.; Donnelly, R.F. A proposed model membrane and test method for microneedle insertion studies. *Int. J. Pharm.* 2014, 472(1-2), 65-73.

[29] Pailler-Mattei, C.; Bec, S.; Zahouani, H. In vivo measurements of the elastic mechanical properties of human skin by indentation tests. *Med. Eng. Phys.* 2008, 30, 599–606.

[30] Gittard, S.D.; Chen, B.; Xu, H.; Ovsianikov, A.; Chichkov, B.N.; Monteiro-Riviere, N.A.; Narayan, R.J. The Effects of Geometry on Skin Penetration and Failure of Polymer Microneedles. *J. Adhes. Sci. Technol*. 2013, 27, 227–243.

[31] Qiu, Y.; Qin, G.; Zhang, S.; Wu, Y.; Xu, B.; Gao, Y. Novel lyophilized hydrogel patches for convenient and effective administration of microneedle-mediated insulin delivery. *Int. J. Pharm*. 2012, 437, 51-56.

[32] Chen, M.C.; Huang, S.F.; Lai, K.Y; Ling, M.H. Fully embeddable chitosan microneedles as a sustained release depot for intradermal vaccination. *Biomaterials* 2013, 34, 3077-3086.

[33] Vemulapalli, V.; Yang, Y.; Friden, P.M.; Banga, A.K. Synergistic effect of iontophoresis and soluble microneedles for transdermal delivery of methotrexate. *J. Pharm. Pharmacol*. 2008, 60, 27-33.

[34] Juluri, A.; Modepalli, N.; Jo, S.; Repka, M.A.; Shivakumar, H.N.; Murthy S.N. Minimally invasive transdermal delivery of iron–dextran. *J. Pharm. Sci.* 2013, 102, 987-993.

[35] Hartkopf, A.D.; Bossow, S.; Lampe, J.; Zimmermann, M.; Taran, F.A.; Wallwiener, D.; Fehm, T.; Bitzer, M.; Lauer, U.M. Enhanced killing of ovarian carcinoma using oncolytic measles vaccine virus armed with a yeast cytosine deaminase and uracil phosphoribosyl transfer. *Gynecol. Oncol.* 2013, 130, 362-368.